PHYSICAL REVIEW D **87,** 034509 (2013)

Nucleon strange quark content from $N_f = 2 + 1$ lattice QCD with exact chiral symmetry

H. Ohki,[1] K. Takeda,[2] S. Aoki,[3,4] S. Hashimoto,[2,5] T. Kaneko,[2,5] H. Matsufuru,[6] J. Noaki,[2] and T. Onogi[7]

(JLQCD Collaboration)

[1]*Kobayashi-Maskawa Institute for the Origin of Particles and the Universe (KMI), Nagoya University, Nagoya, Aichi 464-8602, Japan*
[2]*KEK Theory Center, High Energy Accelerator Research Organization (KEK), Tsukuba 305-0801, Japan*
[3]*Graduate School of Pure and Applied Sciences, University of Tsukuba, Tsukuba, Ibaraki 305-8571, Japan*
[4]*Center for Computational Sciences, University of Tsukuba, Tsukuba, Ibaraki 305-8577, Japan*
[5]*School of High Energy Accelerator Science, The Graduate University for Advanced Studies (Sokendai), Tsukuba 305-0801, Japan*
[6]*Computing Research Center, High Energy Accelerator Research Organization (KEK), Tsukuba 305-0801, Japan*
[7]*Department of Physics, Osaka University, Toyonaka 560-0043, Japan*
(Received 21 August 2012; published 15 February 2013)

We calculate the strange quark content of the nucleon $\langle N|\bar{s}s|N\rangle$ in 2 + 1 -flavor lattice QCD. Chirally symmetric overlap fermion formulation is used to avoid the contamination from up and down quark contents due to an operator mixing between strange and light scalar operators, $\bar{s}s$ and $\bar{u}u + \bar{d}d$. At a lattice spacing $a = 0.112(1)$ fm, we perform calculations at four values of degenerate up and down quark masses m_{ud}, which cover a range of the pion mass $M_\pi \simeq 300$–540 MeV. We employ two different methods to calculate $\langle N|\bar{s}s|N\rangle$. One is a direct method where we calculate $\langle N|\bar{s}s|N\rangle$ by directly inserting the $\bar{s}s$ operator. The other is an indirect method where $\langle N|\bar{s}s|N\rangle$ is extracted from a derivative of the nucleon mass in terms of the strange quark mass. With these two methods we obtain consistent results for $\langle N|\bar{s}s|N\rangle$ with each other. Our best estimate $f_{T_s} = m_s\langle N|\bar{s}s|N\rangle/M_N = 0.009(15)_{\rm stat}(16)_{\rm sys}$ is in good agreement with our previous studies in two-flavor QCD.

DOI: 10.1103/PhysRevD.87.034509 PACS numbers: 11.15.Ha, 12.38.Gc, 14.20.Dh

I. INTRODUCTION

The bulk of the nucleon mass M_N is produced by dynamically broken chiral symmetry in the vacuum of quantum chromodynamics (QCD). This should happen even in the limit of vanishing up and down (current) quark masses. Yet, there are also contributions from nonzero bare masses of up, down, and strange quarks, that are given by a matrix element $m_q\langle N|\bar{q}q|N\rangle$ of a scalar operator $\bar{q}q$ made of quark field q with mass m_q evaluated on the nucleon state $|N\rangle$. This quantity is of fundamental importance to characterize the nucleon structure. More recently, this quantity, especially that of strange quark, is attracting further interest as it determines the cross section of possible dark matter particles to hit the nucleus and thus to determine the sensitivity of dark matter search experiments (see, for instance, Ref. [1]).

The fraction of nucleon mass made of nonvanishing quark masses is conveniently parametrized as

$$f_{T_q} = \frac{m_q\langle N|\bar{q}q|N\rangle}{M_N}. \tag{1}$$

The light quark contents $f_{T_{\{u,d\}}}$ can be related to the πN sigma term $\sigma_{\pi N}$, which is determined from experimental data of the πN scattering amplitude. Evaluation of the strange quark content f_{T_s} is more involved. One uses $\sigma_{\pi N}$ and a phenomenological estimate of the flavor SU(3) violation parameter $\sigma_0 = m_{ud}\langle N|\bar{u}u + \bar{d}d - 2\bar{s}s|N\rangle$, where m_{ud} is (degenerate) up and down quark mass. Recent experimental data $\sigma_{\pi N} = 64(7)$ MeV [2] and $\sigma_0 = 36(7)$ MeV obtained from heavy baryon chiral perturbation theory (HBChPT) [3] led to $f_{T_s} = 0.41(9)$. This large value appeared to be puzzling, as it suggests that the strange quark plays major role to construct nucleon. Early lattice calculations [4–6] also suggested such large value.

In our previous studies [7,8], we carried out nonperturbative calculations of $\langle N|\bar{s}s|N\rangle$ in two-flavor QCD, where up and down quarks are assumed to be degenerate. In Ref. [7], $\langle N|\bar{s}s|N\rangle$ is indirectly estimated from the m_s dependence of M_N through the Feynman-Hellmann theorem

$$\frac{\partial M_N}{\partial m_s} = \langle N|\bar{s}s|N\rangle. \tag{2}$$

We refer to this method as the spectrum method in this paper. In Ref. [8], on the other hand, $\langle N|\bar{s}s|N\rangle$ is extracted directly from a disconnected three-point function of the nucleon (Fig. 1). Since we use a ratio of the three- and two-point functions [see (27) in Sec. III] to improve the accuracy of $\langle N|\bar{s}s|N\rangle$, this method is referred to as the ratio method in the following. These two studies consistently yielded $f_{T_s} \lesssim 0.05$ which is significantly smaller than the phenomenological estimate.

In this paper, we extend our previous studies to 2 + 1-flavor QCD. This is a necessary step towards a

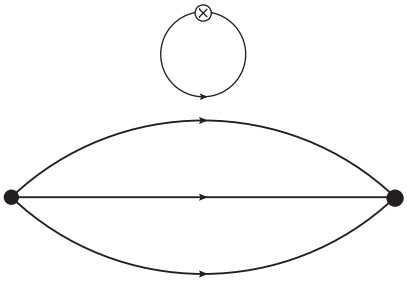

FIG. 1. Nucleon three-point function used to determine $\langle N|\bar{s}s|N\rangle$. Solid lines represent quark propagators that are dressed by gluons and sea quarks. Connected three lines form the nucleon propagator, whereas the disconnected quark loop arises from the strange scalar operator $\bar{s}s$.

realistic calculation of $\langle N|\bar{s}s|N\rangle$, since effects of dynamical strange quarks are difficult to estimate analytically. In addition, we can eliminate a subtlety in the spectrum method when used for two-flavor QCD. Namely, since this theory does not have strange sea quark, we estimated $\langle N|\bar{s}s|N\rangle$ as a derivative in terms of up and down sea quark mass at sea ($m_{ud,\mathrm{sea}}$) and valence ($m_{ud,\mathrm{val}}$) quark masses set to the physical strange quark mass $m_{s,\mathrm{phys}}$

$$\langle N|\bar{s}s|N\rangle = \frac{\partial M_N}{\partial m_{ud,\mathrm{sea}}}\bigg|_{m_{ud,\mathrm{sea}}=m_{ud,\mathrm{val}}=m_{s,\mathrm{phys}}}, \tag{3}$$

assuming that $\langle N|\bar{s}s|N\rangle$ mildly depends on the quark masses. This assumption is eliminated in the present work.

A number of lattice studies of the strange quark content have been recently performed in $N_f = 2$ [9–11], $2+1$ [12–19], and $2+1+1$ [18,20] QCD using either the spectrum [9,12,16,17,19] or ratio [10,11,13–15,18,20] method. An important advantage of our work over the previous calculations is that chiral symmetry is preserved by employing the overlap quark action [21,22]. Conventional Wilson-type fermions, which explicitly violate chiral symmetry at finite lattice spacings, induce a mixing of scalar operators between $\bar{s}s$ and $\bar{u}u + \bar{d}d$ [8]. The nucleon three-point function in Fig. 1 then receives a contribution from a connected diagram with the $\bar{u}u + \bar{d}d$ operator through the renormalization of $\bar{s}s$. The connected contribution is larger than the disconnected one typically by an order of magnitude, and a subtraction of such a large contamination gives rise to a substantial uncertainty in $\langle N|\bar{s}s|N\rangle$ [9]. This serious problem is entirely avoided in our work using the chiral lattice fermion formulation.

This paper is organized as follows. We describe our simulation setup to generate gauge ensembles and to calculate relevant nucleon correlators in Sec. II. The strange quark content is extracted through the ratio and spectrum methods at simulated quark masses in Sec. III. We then extrapolate these results to the physical point in Sec. IV. Our conclusions are given in Sec. V. Our preliminary reports of this work are found in Refs. [23,24].

II. SIMULATION METHOD

A. Gauge ensembles

We simulate QCD with degenerate up and down quarks and heavier strange quarks. Chiral symmetry is exactly preserved by employing the overlap quark action [21,22]. Its Dirac operator is given by

$$D(m) = \left(m_0 + \frac{m}{2}\right) + \left(m_0 - \frac{m}{2}\right)\gamma_5 \mathrm{sgn}[H_W(m_0)], \tag{4}$$

where m is the quark mass and $H_W = \gamma_5 D_W$ is the Hermitian Wilson-Dirac operator. The mass parameter of H_W is chosen as $m_0 = -1.6$ so that the overlap-Dirac operator $D(m)$ has good locality [25]. For gauge fields, we use the Iwasaki action [26] with a modification proposed in Ref. [27]. This leads to an extra Boltzmann factor $\det[H_W^2]/\det[H_W^2 + \mu^2]$ ($\mu = 0.2$), which does not change the continuum limit of the theory but remarkably reduces the computational cost to calculate $\mathrm{sgn}[H_W]$ in (4) by suppressing (near-)zero modes of H_W. This Boltzmann factor prohibits tunnelings among different topological sectors, and we simulate only trivial topological sector in this study. The effect of fixing topology is suppressed by inverse power of the lattice volume [28] and turned out to be small, typically 1% level, in our previous studies [29,30]. This small effect can be safely neglected with our statistical accuracy for baryon observables.

Our gauge ensembles are generated at a gauge coupling $\beta = 2.3$, where the lattice spacing is determined as $a = 0.112(1)$ fm using the Ω baryon mass as input. On a $N_s^3 \times N_t = 16^3 \times 48$ lattice, we simulate two values of the degenerate up and down quark masses $m_{ud} = 0.035$ and 0.050, and two strange quark masses $m_s = 0.080$ and 0.100. Their physical values $m_{ud,\mathrm{phys}} = 0.0029$ and $m_{s,\mathrm{phys}} = 0.081$ are fixed by using M_π and M_K as inputs [30]. Note also that we quote bare values in lattice units for these quark masses. We push our simulations to two smaller m_{ud}'s, 0.015 and 0.025, on a larger lattice $24^3 \times 48$ at a single value of $m_s = 0.080$, which is very close to $m_{s,\mathrm{phys}}$.

Four values of m_{ud} cover a range of the pion mass $M_\pi \simeq$ 300–540 MeV. The spatial extent L is chosen to satisfy a condition $M_\pi L \gtrsim 4$ to control finite volume effects.

TABLE I. Summary of parameters used in the lattice simulation.

m_{ud}	0.015			0.025			0.035		0.050	
m_s	0.080	0.080	0.100	0.080	0.080	0.100	0.080	0.100	0.080	0.100
L/a	24	16	16	24	16	16	16	16	16	16

We carry out additional simulations at the two smallest m_{ud}'s on the smaller lattice size $16^3 \times 48$ to directly examine the finite volume effects. Our simulation parameters are summarized in Table I.

The statistical samples at each simulation point (m_{ud}, m_s, L) consist of 2,500 hybrid Monte Carlo trajectories, out of which we use 500 and 50 to calculate the correlation functions in the spectrum and ratio methods, respectively. We employ the jackknife method with a bin size of 50 trajectories to estimate statistical errors of the nucleon correlators and any quantities determined from them.

On these gauge ensembles, we calculate the two-point nucleon correlation function using an interpolating operator $N = \epsilon^{abc}(u_a^T C\gamma_5 d_b)u_c$ with $C = \gamma_4\gamma_2$. After taking contractions, we obtain

$$\langle C_{2\mathrm{pt}}(\mathbf{y}, t, \Delta t)\rangle = -\frac{1}{2N_s^3}\sum_{\Gamma=(1\pm\gamma_4)/2}\sum_{\mathbf{x}}\epsilon^{abc}\epsilon^{a'b'c'}\langle \mathrm{tr}_s[\Gamma(D^{-1}(m))^{aa'}]\mathrm{tr}_s[\Gamma(D^{-1}(m))^{bb'}(C\gamma_5)((D^{-1}(m))^{cc'})^T(C\gamma_5)] + \mathrm{tr}_s[\Gamma(D^{-1}(m))^{aa'}(C\gamma_5)((D^{-1}(m))^{cc'})^T(C\gamma_5)(D^{-1}(m))^{bb'}]\rangle, \quad (5)$$

where the trace "tr_s" is over spinor indices and $\langle\cdots\rangle$ represents a Monte Carlo average. Here, the quark propagators $D^{-1}(m)$ propagate from $(\mathbf{y}, t)$ to $(\mathbf{x}, t + \Delta t)$. In order to improve statistical accuracy, $C_{2\mathrm{pt}}$ is averaged over two choices of the projector $\Gamma = (1 \pm \gamma_4)/2$, which correspond to the forward and backward propagating nucleons, respectively. Here and in the following, for $\Gamma = (1 - \gamma_4)/2$, Δt is taken as $-\Delta t$.

We also calculate the three-point function with a scalar operator on the lattice defined as

$$\mathcal{O}_S^{\mathrm{lat}} = \bar{s}\left(1 - \frac{D(0)}{2m_0}\right)s \quad (6)$$

to respect chiral symmetry in the continuum limit.

B. All-to-all propagator

As shown in Fig. 1, the three-point function $C_{3\mathrm{pt}}$ on a given gauge configuration can be decomposed into two pieces. Namely, we can write $C_{3\mathrm{pt}}$ as

$$\langle C_{3\mathrm{pt}}(\mathbf{y}, t, \Delta t, \Delta t_s)\rangle = \langle C_{2\mathrm{pt}}(\mathbf{y}, t, \Delta t)S^{\mathrm{lat}}(t + \Delta t_s)\rangle, \quad (7)$$

where $C_{2\mathrm{pt}}(\mathbf{y}, t, \Delta t)$ is the two-point function and

$$S^{\mathrm{lat}}(t + \Delta t_s) = \frac{1}{N_s^3}\sum_{\mathbf{z}}\{\mathrm{Tr}(D^{-1}(m))(z, z)|_{z_0=t+\Delta t_s} - \langle \mathrm{Tr}(D^{-1}(m))(z, z)|_{z_0=t+\Delta t_s}\rangle\}, \quad (8)$$

is the scalar quark loop calculated on this configuration. The trace "Tr" is over both spinor and color indices. The nucleon piece $C_{2\mathrm{pt}}$ can be calculated by using the conventional "point-to-all" quark propagator $D^{-1}(x, x')$, the source point of which (x') has to be fixed to a certain lattice site. The calculation of the quark-loop pieces S^{lat} is computationally more demanding, as it involves quark loops starting from arbitrary lattice sites $(\mathbf{z}, t + \Delta t_s)$. We therefore employ the "all-to-all" quark propagator [31,32] that contains the quark propagating from any lattice site to any site.

Let us consider a decomposition of the quark propagator to the contribution from low-lying eigenmodes of the Dirac operator $D(m)$ and that from the remaining modes

$$D^{-1}(m) = \{D^{-1}(m)\}_{\mathrm{low}} + \{D^{-1}(m)\}_{\mathrm{high}}. \quad (9)$$

It is expected that the low-mode contribution $\{D^{-1}(m)\}_{\mathrm{low}}$ dominates low-energy observables in QCD including $\langle N|\bar{s}s|N\rangle$. We calculate it exactly as

$$\{D^{-1}(m)\}_{\mathrm{low}}(x, y) = \sum_{k=1}^{N_e}\frac{1}{\lambda_k(m)}v_k(x)v_k(y)^\dagger, \quad (10)$$

where $\lambda_k(m)$ and $v_k(x)$ are the kth lowest eigenvalue and its associated eigenvector of $D(m)$, and N_e is the number of the low-lying modes prepared for this calculation.

The small contribution from the remaining high-modes is calculated stochastically by the noise method [33]. We generate a single complex Z_2 noise vector $\eta(x)$ for each configuration and split it into $N_d = 3 \times 4 \times N_t/2$ vectors $\eta^{(d)}(x)$ $(d = 1, \ldots, N_d)$, which have nonzero elements only for a single combination of color and spinor indices on two consecutive time slices. For each "split" noise vector $\eta^{(d)}$, we solve a linear equation

$$\{D(m)\psi^{(d)}\}(x) = (\mathcal{P}_{\mathrm{high}}\eta^{(d)})(x) \quad (d = 1, \ldots, N_d), \quad (11)$$

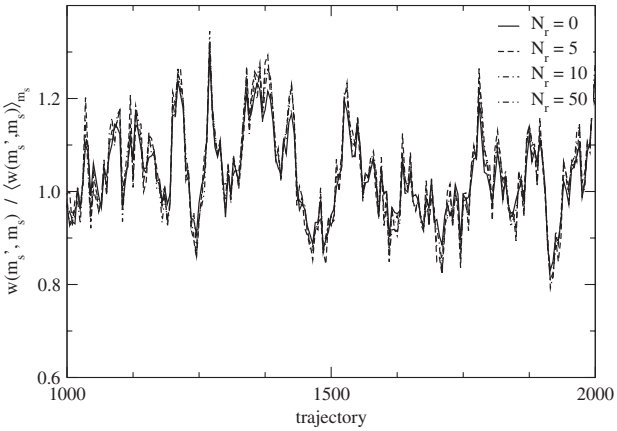

FIG. 2. Monte Carlo history of reweighting factor $\tilde{w}(m_s', m_s)$ to shift the strange quark mass from $m_s' = 0.080$ to $m_s = 0.075$ at $m_{ud} = 0.050$. Different lines show data calculated with different numbers of the pseudofermion fields N_r.

where $\mathcal{P}_{\rm high} = 1 - \mathcal{P}_{\rm low}$ and $\mathcal{P}_{\rm low}$ is the projector to the subspace spanned by the low-modes

$$\mathcal{P}_{\rm low}(x, y) = \sum_{k=1}^{N_e} v_k(x) v_k(y)^\dagger. \tag{12}$$

The high-mode contribution is then estimated as

$$\{D^{-1}(m)\}_{\rm high}(x, y) = \sum_{d=1}^{N_d} \psi^{(d)}(x) \eta^{(d)}(y)^\dagger. \tag{13}$$

We calculate the low- and high-mode contributions to $S^{\rm lat}$ as

$$S^{\rm lat}(t + \Delta t_s) = S^{\rm lat}_{\rm low}(t + \Delta t_s) + S^{\rm lat}_{\rm high}(t + \Delta t_s), \tag{14}$$

with

$$S^{\rm lat}_{\rm low(high)}(t + \Delta t_s) = \frac{1}{N_s^3} \sum_{\mathbf{z}} \{D^{-1}(m)\}_{\rm low(high)}(z, z)|_{z_0 = t + \Delta t_s}, \tag{15}$$

where the subtraction of the vacuum expectation value is assumed though it is not written explicitly for notational simplicity.

C. Low-mode averaging (LMA)

The low-lying modes of $D(m)$ are also useful to precisely calculate the nucleon piece $C_{\rm 2pt}$ in both $C_{\rm 2pt}$ and $C_{\rm 3pt}$. By applying (9), we can decompose $C_{\rm 2pt}$ into the following eight contributions:

$$C_{\rm 2pt} = C^{lll}_{\rm 2pt} + C^{llh}_{\rm 2pt} + C^{lhl}_{\rm 2pt} + C^{hll}_{\rm 2pt} + C^{lhh}_{\rm 2pt} + C^{hlh}_{\rm 2pt} + C^{hhl}_{\rm 2pt} + C^{hhh}_{\rm 2pt}. \tag{16}$$

Here, $C^{lll}_{\rm 2pt}$ is constructed only from $\{D^{-1}(m)\}_{\rm low}$. For $C^{llh}_{\rm 2pt}$, $\{D^{-1}(m)\}_{\rm low}$ is used for two of the valence quark propagators and $\{D^{-1}(m)\}_{\rm high}$ for the remaining one. The other combinations are understood in a similar manner. In principle, we can use the all-to-all propagator, (10) and (13), to calculate these contributions. These quantities, however, decay exponentially with a large nucleon mass M_N as the temporal separation Δt increases. At large separations, the high-mode contributions, such as $C^{hhh}_{\rm 2pt}$, are not sufficiently precise with $\{D^{-1}(m)\}_{\rm high}$ evaluated using only single noise sample for each configuration.

We therefore use the low-mode averaging (LMA) technique [34,35] in this study. The low-mode part of the

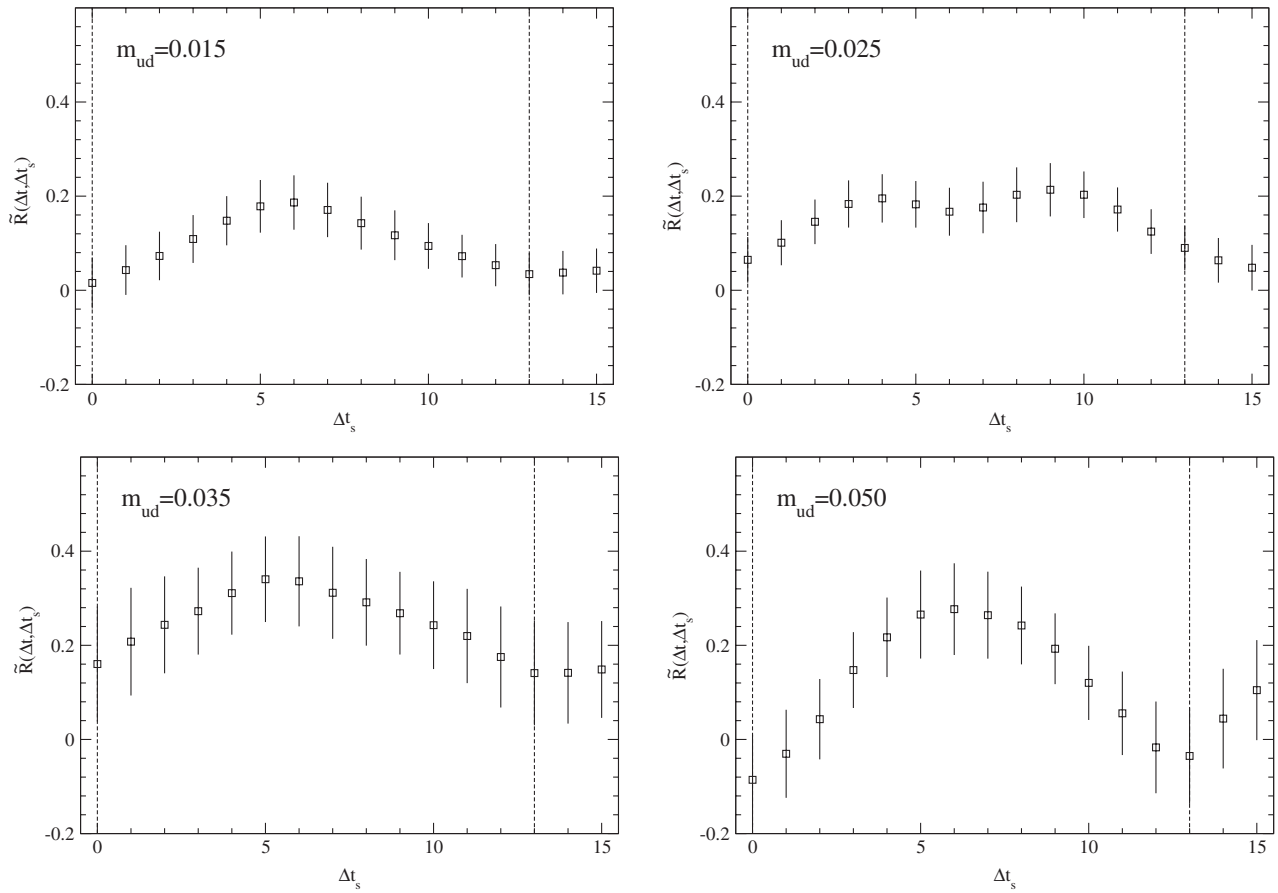

FIG. 3. Approximated ratio $\tilde{R}(\Delta t, \Delta t_s)$ at $m_s = 0.080$ as a function of Δt_s. We plot results obtained at different values of m_{ud} in the four panels. The vertical dashed lines show the locations of the nucleon source and sink operators.

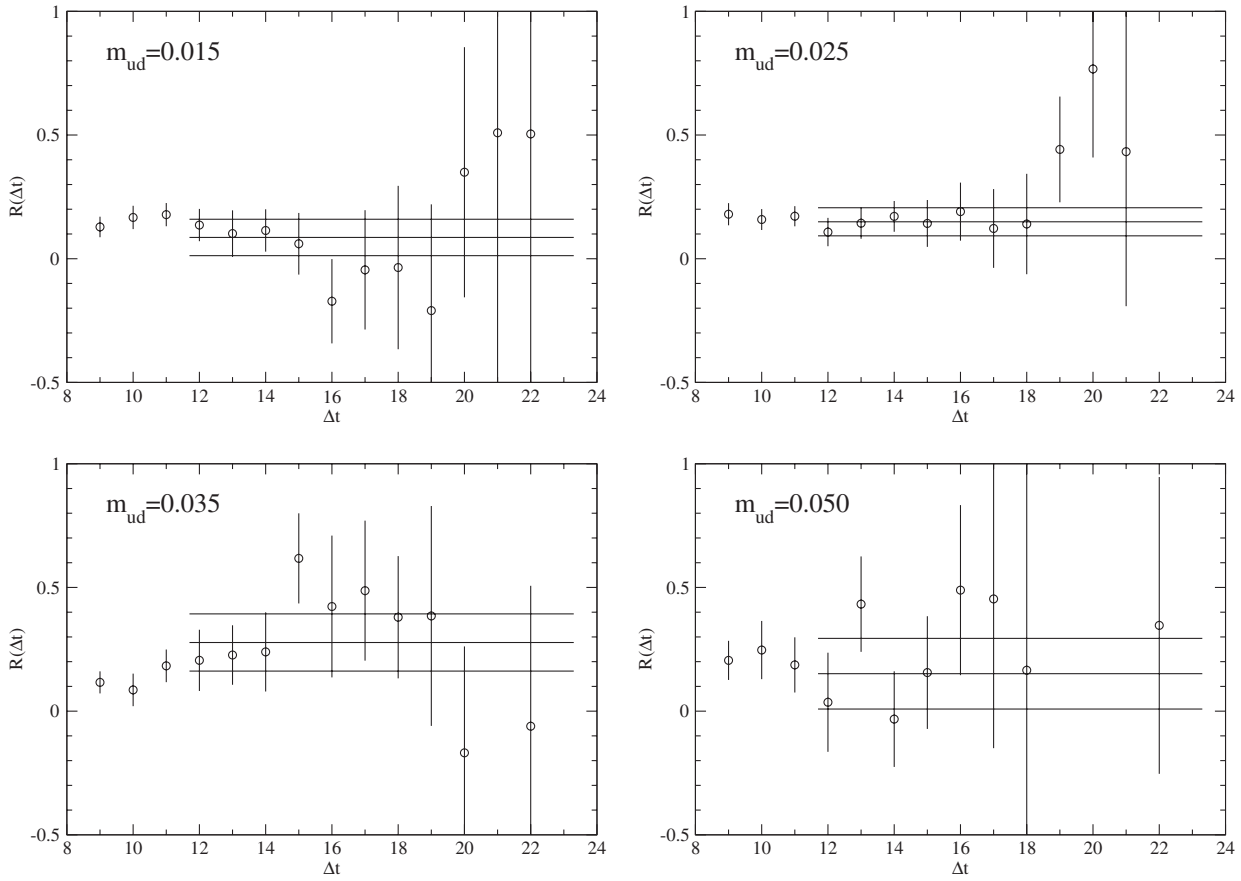

FIG. 4. Results of the constant fit to $R(\Delta t, \Delta t_s)$ as a function of Δt. Four panels show results obtained at different values of m_{ud} and at $m_s = 0.080$.

all-to-all propagator (10) is used to calculate $C^{lll}_{\rm 2pt}$, which dominantly contributes to the nucleon correlators $C_{\rm 2pt}$ and $C_{\rm 3pt}$. We then take average of $C^{lll}_{\rm 2pt}(\mathbf{y}, t, \Delta t)$ over the location of the nucleon source operator $(\mathbf{y}, t)$ to largely reduce its statistical fluctuation.

The remaining and small contributions $\{C^{llh}_{\rm 2pt}, \ldots, C^{hhh}_{\rm 2pt}\}$ are calculated using the point-to-all quark propagator after projecting by $\mathcal{P}_{\rm low}$ and $1 - \mathcal{P}_{\rm low}$ for l and h pieces, respectively. We improve the statistical signal of these contributions by averaging over $(\mathbf{y}, t)$. In order to reduce the computational cost of the re-calculation of the point-to-all propagators, these contributions are averaged over a limited set of $(\mathbf{y}, t)$ compared to that for $C^{lll}_{\rm 2pt}$.

The sets of the source point as well as the number of the low-modes N_e are chosen differently for our calculations with the ratio and spectrum methods, because the latter uses $C_{\rm 2pt}$ calculated in the course of our study of the light meson spectrum [29,30]. We summarize our choices for these two methods in the following subsections.

D. Setup for the ratio method

We use $N_e = 160$ and 240 low-lying modes on the $16^3 \times 48$ and $24^3 \times 48$ lattices, respectively, to calculate low-mode contribution $S^{\rm lat}_{\rm low}(t + \Delta t)$ and $C^{lll}_{\rm 2pt}(\mathbf{y}, t, \Delta t)$ in the ratio method. As mentioned above, the latter is averaged over 16 spatial points

$$\mathbf{y} \in \{(0,0,0), (0,0,N_s/2), (0,N_s/2,N_s/2), (N_s/2,N_s/2,N_s/2), (N_s/4,N_s/4,N_s/4), (N_s/4,N_s/4,3N_s/4), (N_s/4,3N_s/4,3N_s/4), (3N_s/4,3N_s/4,3N_s/4), \text{and their permutations}\} \quad (17)$$

TABLE II. Strange quark content $\langle N|\mathcal{O}^{\rm lat}_S|N\rangle$ calculated in the ratio method.

m_{ud}	0.015	0.025	0.035	0.035	0.050	0.050
m_s	0.080	0.080	0.080	0.100	0.080	0.100
$\langle N|\mathcal{O}^{\rm lat}_S|N\rangle$	0.09(7)	0.15(6)	0.28(12)	0.14(10)	0.15(14)	0.20(18)

TABLE III. Same as Table II but for $m_{ud} = 0.015$ and 0.025 on the smaller volume $16^3 \times 48$.

m_{ud}	0.015	0.015	0.025	0.025
m_s	0.080	0.100	0.080	0.100
$\langle N \vert \mathcal{O}_S^{\rm lat} \vert N \rangle$	0.34(24)	0.29(32)	0.21(16)	0.02(9)

at each time slice t. Averaging over more points does not help to further reduce the statistical fluctuation of $C_{2\rm pt}$ and $C_{3\rm pt}$ because of the correlation among $C_{2\rm pt}^{lll}(\mathbf{y}, t, \Delta t)$ at different spatial points $\mathbf{y}$'s. We average $\{C_{2\rm pt}^{llh}, \ldots, C_{2\rm pt}^{hhh}\}$ over four time slices $t = 0$, 12, 24, and 36 with the spatial location $\mathbf{y}$ kept fixed.

At heaviest $m_{ud}(= 0.050)$, we slightly modify the setup of LMA to calculate $C_{3\rm pt}$. With (14) and (16), $C_{3\rm pt}$ on a given configuration can be rewritten as

$$C_{3\rm pt} = C_{2\rm pt}^{lll} S_{\rm low}^{\rm lat} + \{C_{2\rm pt}^{llh} + \cdots + C_{2\rm pt}^{hhh}\} S_{\rm low}^{\rm lat} + C_{2\rm pt}^{lll} S_{\rm high}^{\rm lat} + \{C_{2\rm pt}^{llh} + \cdots + C_{2\rm pt}^{hhh}\} S_{\rm high}^{\rm lat}. \quad (18)$$

The first term represents the low-mode contribution, which gives a dominant contribution to $C_{3\rm pt}$ especially for small m_{ud}. Other three terms are relatively minor contributions, and their statistical fluctuation is not substantially reduced by LMA. At the largest m_{ud}, the statistical error becomes even larger when LMA is used. We therefore apply LMA only for the first term in that case.

The above setup of LMA typically leads to a factor of 4 (7) reduction of the statistical error of $C_{2\rm pt}$ ($C_{3\rm pt}$) at our simulated values of m_{ud} and m_s.

In our previous study in two-flavor QCD [8], we observe that smearing both nucleon source and sink operators is crucial to identify the ground state contribution to $C_{3\rm pt}$. We employ the Gaussian smearing

$$q_{\rm smr}^{\rm gss}(\mathbf{x}, t) = \sum_{\mathbf{y}} \left\{ \left(\mathbb{1} + \frac{\omega}{4N} H \right)^N \right\}_{\mathbf{x},\mathbf{y}} q(\mathbf{y}, t),$$
$$H_{\mathbf{x},\mathbf{y}} = \sum_{i=1}^{3} (\delta_{\mathbf{x},\mathbf{y}-\hat{i}} + \delta_{\mathbf{x},\mathbf{y}+\hat{i}}), \quad (19)$$

where we omit the gauge links connecting the lattice sites $(\mathbf{x}, t)$ and $(\mathbf{y}, t)$, which may enhance the statistical fluctuation of $C_{2\rm pt}$ and $C_{3\rm pt}$. We use this gauge noninvariant smearing on our gauge configurations fixed to the Coulomb gauge. The parameters $\omega = 20$ and $N = 400$ are chosen by inspecting the plateau of the effective mass of $C_{2\rm pt}$.

E. Setup for the spectrum method

For the spectrum method, we use $C_{2\rm pt}$ calculated in the course of our study of the light meson spectrum [29,30]. The low-mode contribution $C_{2\rm pt}^{lll}(\mathbf{y}, t, \Delta t)$ is calculated using $N_e = 160(80)$ low-modes on the $16^3 \times 48$ ($24^3 \times 48$) lattice, and is averaged over the time-slice t with the spatial source point $\mathbf{y}$ kept fixed. We use an exponential smearing

$$q_{\rm smr}^{\rm exp}(\mathbf{x}, t) = \sum_{\mathbf{r}} \exp[-0.4|\mathbf{r}|] q(\mathbf{x} + \mathbf{r}, t) \quad (20)$$

only for the nucleon source operator. The spatial extent of this smeared operator is roughly equal to that of (19) used for the ratio method. We observe that the onset of the plateau in the effective mass is consistent with that of (19) within the statistical error.

In order to evaluate the derivative $\partial M_N / \partial m_s$ in (2), we study the m_s dependence of M_N by utilizing the reweighting technique [36,37]. Our Monte Carlo data at the strange quark mass m_s are used to estimate the two-point function at a slightly shifted strange quark mass m_s' as

$$\langle C_{2\rm pt} \rangle_{m_s'} = \langle C_{2\rm pt} \tilde{w}(m_s', m_s) \rangle_{m_s}, \quad (21)$$

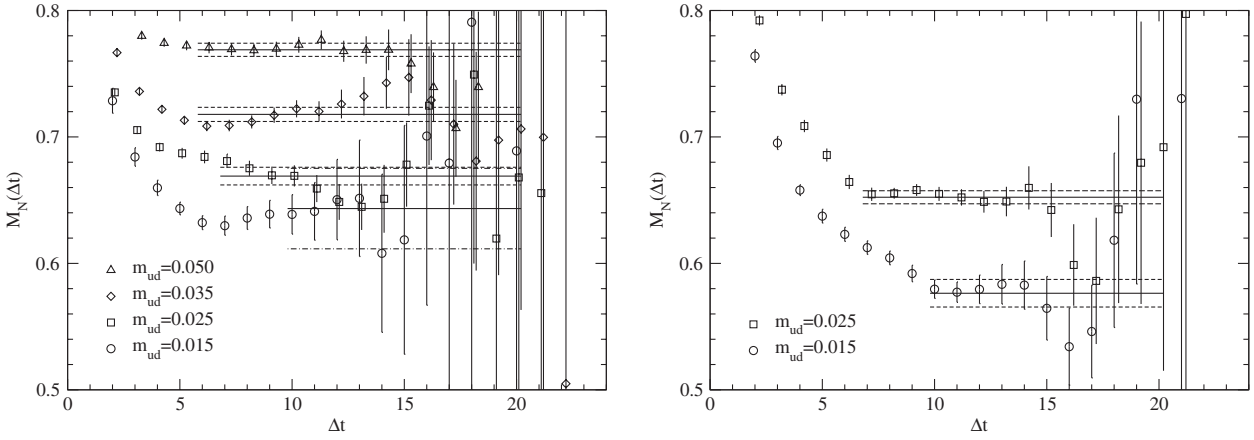

FIG. 5. Nucleon effective masses at $m_s = 0.080$. Left and right panels show results on the $16^3 \times 48$ and $24^3 \times 48$ lattices, respectively. Horizontal lines show M_N obtained from a single exponential fit to $C_{2\rm pt}(\Delta t)$.

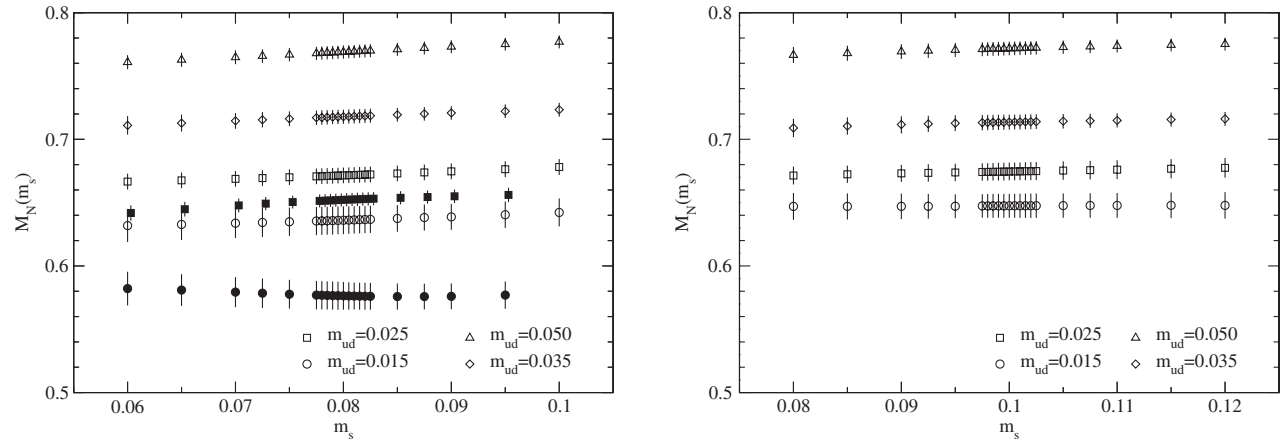

FIG. 6. Nucleon masses M_N as a function of m_s. Left and right panels show M_N obtained by reweighting from that at $m_s = 0.080$ and 0.100, respectively. We plot results on the $16^3 \times 48$ and $24^3 \times 48$ lattices, by open and filled symbols. Filled squares are slightly shifted in the horizontal direction for clarity.

where $\langle \cdots \rangle_{m_s}$ represents the Monte Carlo average at m_s, and $\tilde{w}$ is the reweighting factor for a given configuration

$$\tilde{w}(m_s', m_s) = \frac{w(m_s', m_s)}{\langle w(m_s', m_s)\rangle_{m_s}}, \qquad w(m_s', m_s) = \det\left[\frac{D(m_s')}{D(m_s)}\right]. \tag{22}$$

Similarly to $S^{\rm lat}$ and $C_{\rm 2pt}$, w can be decomposed into contributions from low and high modes

$$w(m_s', m_s) = w_{\rm low}(m_s', m_s) w_{\rm high}(m_s', m_s), \tag{23}$$

$$w_{\rm low(high)}(m_s', m_s) = \det\left[\mathcal{P}_{\rm low(high)} \frac{D(m_s')}{D(m_s)} \mathcal{P}_{\rm low(high)}\right]. \tag{24}$$

We exactly calculate $w_{\rm low}$ using the low-lying eigenvalues, whereas $w_{\rm high}$ is estimated by a stochastic estimator for its square

$$w_{\rm high}^2(m_s', m_s) = \frac{1}{N_r} \sum_{r=1}^{N_r} e^{-\frac{1}{2}(\mathcal{P}_{\rm high}\xi_r)^\dagger(\Omega - 1)\mathcal{P}_{\rm high}\xi_r}. \tag{25}$$

Here $\Omega \equiv D(m_s)^\dagger \{D(m_s')^{-1}\}^\dagger D(m_s')^{-1} D(m_s)$, and $\{\xi_1, \ldots, \xi_{N_r}\}$ is a set of pseudofermion fields whose elements are generated with the Gaussian probability.

An important practical issue is how many pseudofermion fields are needed to reliably estimate $w_{\rm high}$. Since $w_{\rm high}$ is a product of $12N_s^3N_t - N_e$ eigenvalues, it largely deviates from unity unless $m_s \simeq m_s'$. We observe, however, that it has small statistical fluctuation, after taking the ratio $\tilde{w}(m_s', m_s) = w(m_s', m_s)/\langle w(m_s', m_s)\rangle_{m_s}$. Consequently, the normalized reweighting factor $\tilde{w}$ is essentially controlled by the low-mode contribution $w_{\rm low}$. We therefore do not need large number of the pseudofermion fields to estimate $w_{\rm high}$ as demonstrated in Fig. 2.

In this study, we reweight $C_{\rm 2pt}$ at $m_s = 0.080$ to 20 different values

$$\begin{aligned} m_s' = {} & 0.0600, 0.0650, 0.0700, 0.0725, 0.0750, 0.0775, \\ & 0.0780, 0.0785, 0.0790, 0.0795, 0.0805, 0.0810, \\ & 0.0815, 0.0820, 0.0825, 0.0850, 0.0875, 0.0900, \\ & 0.0950, 0.1000. \end{aligned} \tag{26}$$

We shift these values by $+0.020$ when we reweight $C_{\rm 2pt}$ at $m_s = 0.100$. These values roughly cover a region $m_s' \in [m_s - 25\,\text{MeV}, m_s + 25\,\text{MeV}]$, where the low-mode dominance of $\tilde{w}$ is confirmed. We set $N_r = 5$ in the whole region of m_s'.

III. RESULTS AT THE SIMULATED QUARK MASSES

In the following subsections, we present our results for $\langle N|\mathcal{O}_S^{\rm lat}|N\rangle$ obtained at simulated quark masses by using the ratio and spectrum methods. Note that $\langle N|\mathcal{O}_S^{\rm lat}|N\rangle$ represents the bare value on the lattice, and results for the renormalization group invariant parameter f_{T_s} will be given in the next section.

TABLE IV. Strange quark content $\langle N|\mathcal{O}_S^{\rm lat}|N\rangle$ obtained from the spectrum method.

m_{ud}	0.015	0.025	0.035	0.035	0.050	0.050
m_s	0.080	0.080	0.080	0.100	0.080	0.100
$\langle N\|\mathcal{O}_S^{\rm lat}\|N\rangle$	−0.16(35)	0.35(13)	0.31(15)	0.16(12)	0.42(10)	0.22(10)

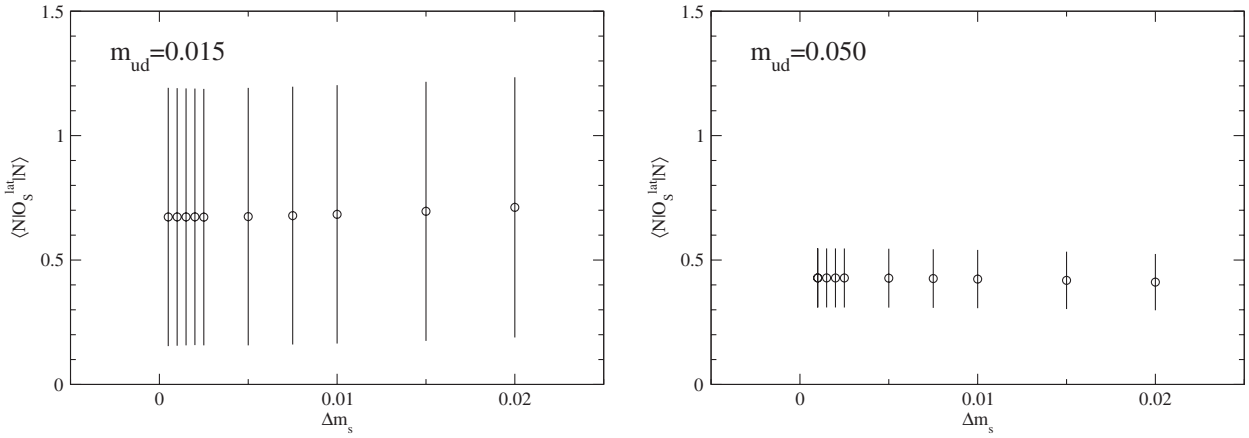

FIG. 7. Fitted results for $\langle N|\mathcal{O}_S^{\rm lat}|N\rangle$ as a function of the width of the fitting range Δm_s. Left and right panels show results at $(m_{ud}, m_s) = (0.015, 0.080)$ and $(m_{ud}, m_s) = (0.050, 0.080)$, respectively.

A. Ratio method

We extract $\langle N|\mathcal{O}_S^{\rm lat}|N\rangle$ from the ratio of $C_{3\rm pt}(\Delta t, \Delta t_s)$ and $C_{2\rm pt}(\Delta t)$

$$R(\Delta t, \Delta t_s) \equiv \frac{C_{3\rm pt}(\Delta t, \Delta t_s)}{C_{2\rm pt}(\Delta t)} \underset{\Delta t, \Delta t_s \to \infty}{\longrightarrow} \langle N|\mathcal{O}_S^{\rm lat}|N\rangle, \qquad (27)$$

where Δt is the temporal interval between the nucleon source and sink. The scalar quark loop $S^{\rm lat}$ is set on the time-slice apart from the nucleon source by Δt_s. Note that $C_{3\rm pt}(\Delta t, \Delta t_s)$ and $C_{2\rm pt}(\Delta t)$ are calculated using LMA and, hence, we suppress the coordinates of the nucleon source, namely, $(\mathbf{y}, t)$ in (5) and (7).

The ratio R may receive contamination from excited states of the nucleon when the temporal separation Δt is not sufficiently large and/or the scalar operator is too close to the nucleon operators ($\Delta t_s \sim 0$ or Δt). We therefore need to identify a plateau of $R(\Delta t, \Delta t_s)$, where the excited state contamination is negligible. To this end, we consider the same ratio but approximated by taking only the low-mode contribution $S_{\rm low}^{\rm lat}$ for the quark loop $S^{\rm lat}$ in (14). This approximated ratio, which we denote by $\tilde{R}$ in the following, is useful to identify the plateau of R, because (i) R is well dominated by the low-mode approximation $\tilde{R}$, and (ii) $\tilde{R}$ is free from a large noise due to the stochastic method to estimate $S_{\rm high}^{\rm lat}$, which obscures the excited state contamination. We refer the reader to Ref. [8] for a more detailed discussion.

Figure 3 shows $\tilde{R}(\Delta t, \Delta t_s)$ with a fixed value of $\Delta t = 13$ as a function of Δt_s. We obtain nonzero signal for $\tilde{R}(\Delta t, \Delta t_s)$, which do not show significant Δt_s dependence at $\Delta t_s \sim \Delta t/2$. It implies that the scalar operator is sufficiently far from nucleon operators.

We then carry out a constant fit to the ratio without the approximation $R(\Delta t, \Delta t_s)$ using a fit range of $\Delta t_s = [5, \Delta t - 5]$ for each Δt. As plotted in Fig. 4, the fit results do not show statistically significant dependence on Δt at $\Delta t \geq 12$, that indicates that the data are dominated by the ground state contribution. Although the statistical signal is worse at $m_{ud} = 0.050$, it is reasonable to assume the ground state saturation at around the same Δt region as other m_{ud}'s.

From these observations on the Δt_s and Δt dependences, we determine $\langle N|\mathcal{O}_S^{\rm lat}|N\rangle$ by a simultaneous constant fit to $R(\Delta t, \Delta t_s)$ with fit ranges of $\Delta t_s = [5, \Delta t - 5]$ and $\Delta t = [12, 23]$. The numerical results are listed in Table II. We also test a fitting form taking account of the first excited state with a slightly wider fit range of Δt_s. This fit yields $\langle N|\mathcal{O}_S^{\rm lat}|N\rangle$ in good agreement with those from the constant fit, because the excited state contribution is small as expected from the mild Δt dependence of $R(\Delta t, \Delta t_s)$.

We repeat the same analysis at two smallest m_{ud}'s but on the smaller volume $16^3 \times 48$. The numerical results are listed in Table III. The difference in $\langle N|\mathcal{O}_S^{\rm lat}|N\rangle$ between the two volumes are well below our statistical accuracy suggesting that finite volume effects (FVEs) can be neglected within the statistical error. We therefore use the numerical results in Table II in the chiral extrapolation to determine $\langle N|\mathcal{O}_S^{\rm lat}|N\rangle$ at physical quark masses.

B. Spectrum method

In the spectrum method, we evaluate $\langle N|\mathcal{O}_S^{\rm lat}|N\rangle$ from the m_s dependence of the nucleon mass M_N. Figure 5 shows examples of the nucleon effective mass obtained at $m_s = 0.080$. By a single exponential fit $C_{2\rm pt}(\Delta t) \propto e^{-M_N \Delta t}$, we determine M_N with an accuracy of 2% (0.8%) at our smallest (largest) m_{ud} on $24^3 \times 48$ ($16^3 \times 48$).

TABLE V. Same as Table IV but at $m_{ud} = 0.015$ and 0.025 on the smaller volume $16^3 \times 48$.

m_{ud}	0.015	0.015	0.025	0.025
m_s	0.080	0.100	0.080	0.100
$\langle N\|\mathcal{O}_S^{\rm lat}\|N\rangle$	0.68(52)	−0.60(55)	0.34(11)	0.12(18)

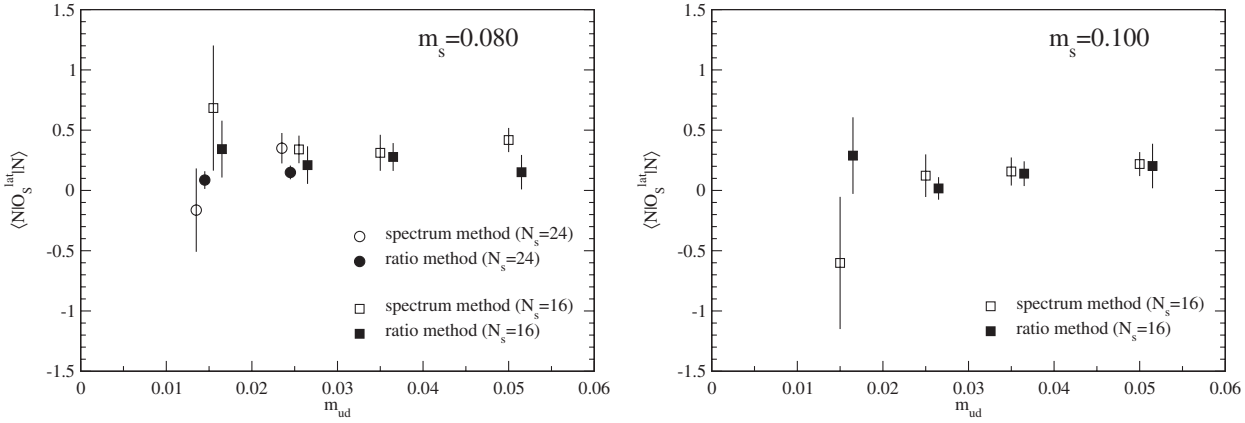

FIG. 8. Strange quark content $\langle N|\mathcal{O}_S^{\rm lat}|N\rangle$ as a function of m_{ud} (given in the lattice unit). Left and right panels show the results from the spectrum and ratio methods, respectively.

The FVE in M_N at $m_{ud} = 0.025$ is not statistically significant: it is only 2σ (3%) effect. We expect similarly small effect at heavier m_{ud}'s. The magnitude of the FVE at $m_{ud} = 0.015$ is difficult to estimate due to a large statistical error of M_N on the smaller volume $16^3 \times 48$. We note that the FVE at $m_{ud} = 0.015$ on the larger volume $24^3 \times 48$ is estimated as 0.7% from $SU(2)$ HBChPT at one-loop. In addition, it is plausible that the FVE has a mild dependence on m_s leading to small effect in $\langle N|\mathcal{O}_S^{\rm lat}|N\rangle$.

As explained in the previous section, we calculate M_N at shifted values of m_s by exploiting the reweighting technique. Results are plotted as a function of m_s in Fig. 6. We successfully reweight our data to $m_s \pm 0.02$ ($\pm$ 25 MeV). Namely, the reweighting does not largely increase the statistical error of M_N. This is because (i) the reweighting factor $\tilde{w}$, is accurately calculated with the small number of the noise samples, as discussed in the previous section, and (ii) resulting values are typically $O(1)$ as plotted in Fig. 2.

We extract the slope $\partial M_N/\partial m_s$ by fitting M_N in the region of $[m_s - \Delta m_s, m_s + \Delta m_s]$ with $\Delta m_s = 0.010$ to a linear form

$$M_N = d + \langle N|\mathcal{O}_S^{\rm lat}|N\rangle m_s. \tag{28}$$

The numerical results are summarized in Table IV. Figure 7 shows that the fitted result for $\langle N|\mathcal{O}_S^{\rm lat}|N\rangle$ is stable against the choice of the fitting range Δm_s as expected from the mild m_s dependence of M_N shown in Fig. 6. We also confirm that adding higher order terms to (28) does not change $\langle N|\mathcal{O}_S^{\rm lat}|N\rangle$ significantly.

In order to directly check FVEs to $\langle N|\mathcal{O}_S^{\rm lat}|N\rangle$, we repeat the analysis at two lightest m_{ud} but on the smaller volume. A comparison with results listed in Table V suggests that FVE is not significant with our statistical accuracy, which is consistent with our observation in the ratio method.

C. Comparison between two methods

Figure 8 compares $\langle N|\mathcal{O}_S^{\rm lat}|N\rangle$ obtained from the spectrum and ratio methods. We observe a good agreement between the two methods. The same figure also shows that FVEs in $\langle N|\mathcal{O}_S^{\rm lat}|N\rangle$ are not significant at the two smallest m_{ud}'s as already mentioned in the previous

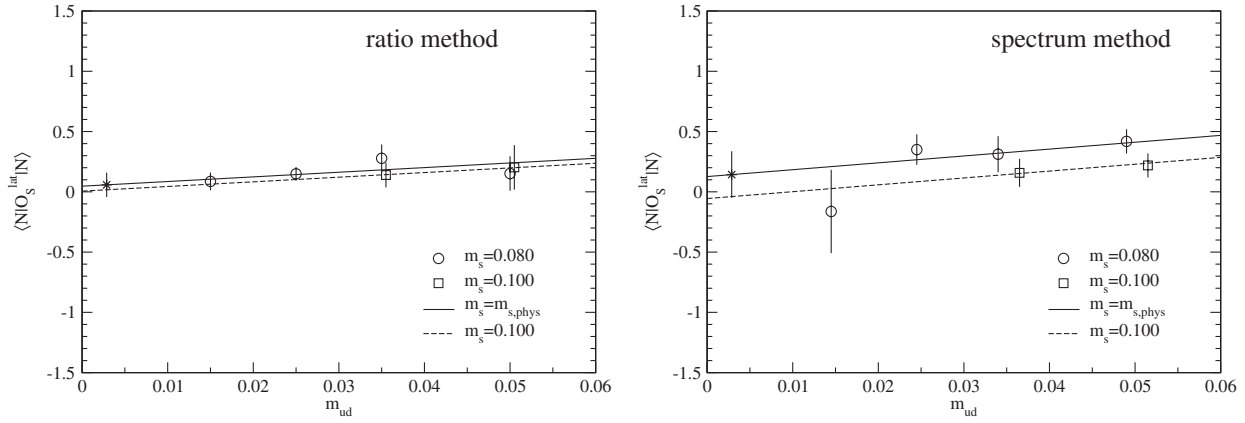

FIG. 9. Linear extrapolations of $\langle N|\mathcal{O}_S^{\rm lat}|N\rangle$ obtained from ratio (left panel) and spectrum (right panel) methods. Solid and dashed lines show the fit lines at $m_s = m_{s,\rm phys}$ and 0.100, respectively. We omit the fit line at $m_s = 0.080$, which is not indistinguishable from that at $m_s = m_{s,\rm phys}$ in the scale of the figure. Star symbols represent $\langle N|\mathcal{O}_S^{\rm lat}|N\rangle$ extrapolated to the physical quark masses. Square symbols are slightly shifted in the horizontal direction for clarity.

TABLE VI. Numerical results of linear chiral extrapolation.

	χ^2/d.o.f.	d.o.f.	c_0	c_1	$c_{1,s}$	$\langle N\|\mathcal{O}_S^{\rm lat}\|N\rangle$
Spectrum method	0.54	3	0.90(47)	5.7(5.1)	−9.6(5.4)	0.15(0.19)
Ratio method	0.38	3	0.22(43)	3.9(4.1)	−2.2(5.7)	0.058(0.101)

subsections. These observations suggest that systematics of our determinations at given quark masses (m_{ud}, m_s) is not substantial.

With our simulation setup, the accuracy at two heaviest m_{ud}'s are comparable between the two methods, while the ratio method provides a more accurate determination at lighter m_{ud}'s. This is mainly because (i) we use the better setup of LMA for the ratio method and (ii) the volume size is increased at these m_{ud}'s. For instance, we average $C_{\rm 2pt}^{lll}(\mathbf{y}, t, \Delta t)$ at the 16 choices of the spatial location $\mathbf{y}$, while $\mathbf{y}$ is kept fixed in the spectrum method. Our data at the 16 choices listed in (17) have less correlation among them on a larger volume and hence LMA works better.

IV. CHIRAL EXTRAPOLATION

In Fig. 9, we plot $\langle N|\mathcal{O}_S^{\rm lat}|N\rangle$ obtained from the two methods as a function of m_{ud}. Note that our data cover a region of $M_\pi \sim 300$–540 MeV, and our lighter strange quark mass $m_s = 0.080$ is already close to the physical mass $m_{s,\rm phys} = 0.081$. The figure shows that $\langle N|\mathcal{O}_S^{\rm lat}|N\rangle$ has a very mild dependence on both m_{ud} and m_s, which has also been observed in our previous study in two-flavor QCD [8]. Our data are well described by a linear fit

$$\langle N|\mathcal{O}_S^{\rm lat}|N\rangle = c_0 + c_{1,ud} m_{ud} + c_{1,s} m_s \tag{29}$$

as plotted in the same figure. Numerical results of the fit are summarized in Table VI. We also confirm that $\langle N|\mathcal{O}_S^{\rm lat}|N\rangle$ at the physical quark masses does not change significantly by excluding the data at the largest m_{ud} from the fit and/or by including higher order terms in (29).

We also test a fitting form based on $SU(3)$ HBChPT to parametrize the observed quark mass dependence of $\langle N|\bar{s}s|N\rangle$. One-loop chiral expansion of M_N [38] and the Feynman-Hellmann theorem (2) give an expression of $\langle N|\mathcal{O}_S^{\rm lat}|N\rangle$

$$\langle N|\mathcal{O}_S^{\rm lat}|N\rangle = -c_s - B\left\{\frac{3}{2} C_{NNK} M_K + 2 C_{NN\eta} M_\eta\right\} + c_{2,K} M_K^2 + c_{2,\eta} M_\eta^2, \tag{30}$$

where contributions of the decuplet baryons are ignored. In this analysis, we approximate the higher order corrections by the $O(M_{\{K,\eta\}}^2)$ analytic terms. Within this approximation, we can use the leading order expressions $M_K^2 = B(m_{ud} + m_s)$ and $M_\eta^2 = 2B(m_{ud} + 2m_s)/3$ for the meson masses. The coefficients C_{NNK} and $C_{NN\eta}$ of the $O(M_{\{K,\eta\}})$ terms are written as

$$C_{NNK} = \frac{1}{8\pi f^2}\frac{(5D^2 - 6DF + 9F^2)}{3}, \qquad C_{NN\eta} = \frac{1}{8\pi f^2}\frac{(D - 3F)^2}{6}. \tag{31}$$

The axial couplings are fixed to a phenomenological estimate $D = 0.81$ and $F = 0.47$ [39] in this analysis. The low-energy constants in mesonic ChPT, f and B, are set to our lattice estimate determined from the meson spectrum and decay constants [30].

The fit using (30) is shown in Fig. 10. Since $\langle N|\bar{s}s|N\rangle$ depends mildly on m_{ud} through the strange meson masses $M_{\{K,\eta\}}$ up to one-loop order of HBChPT, the mild m_{ud} dependence of our data can be fitted to (30) reasonably well. However, numerical results summarized in Table VII suggest a large difference of $\langle N|\mathcal{O}_S^{\rm lat}|N\rangle$ in the $SU(3)$ chiral limit between the linear and HBChPT fits (cf., $-c_s$ in

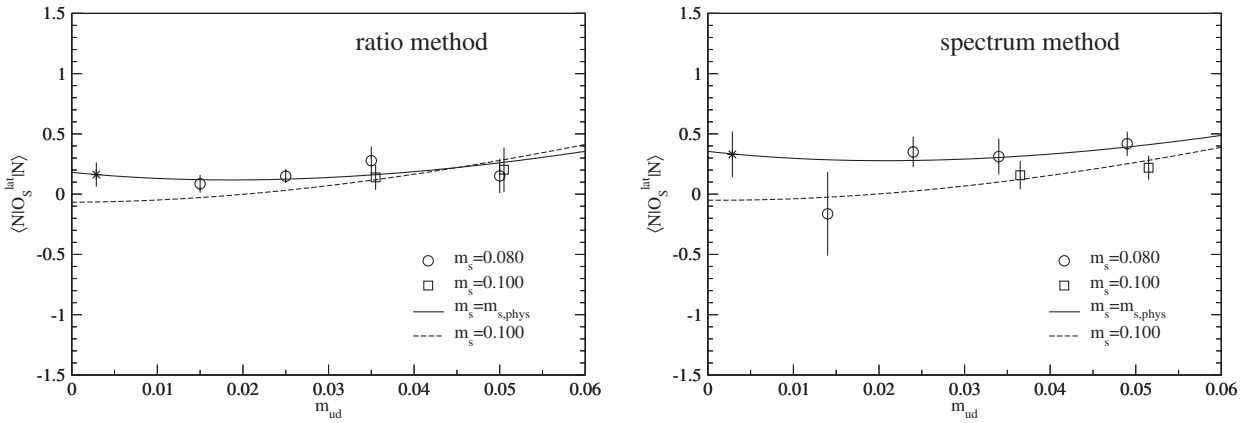

FIG. 10. Chiral fits of $\langle N|\mathcal{O}_S^{\rm lat}|N\rangle$ using $SU(3)$ HBChPT (30). Left and right panels show fits to $\langle N|\mathcal{O}_S^{\rm lat}|N\rangle$ obtained from the ratio and spectrum methods, respectively.

TABLE VII. Numerical results of chiral fit using $SU(3)$ HBChPT (30).

	χ^2/d.o.f.	d.o.f.	$-c_s$	$c_{2,K}$ [GeV^{-2}]	$c_{2,\eta}$ [GeV^{-2}]	$\langle N\|\mathcal{O}_S^{\rm lat}\|N\rangle$
Spectrum method	1.2	3	8.7(5)	23(4)	−6.1(3.6)	0.33(19)
Ratio method	0.75	3	7.9(4)	21(3)	−2.8(3.6)	0.16(10)

Table VII and c_0 in Table VI). This is because (30) predicts a large $O(M_K)$ contribution to $\langle N|\mathcal{O}_S^{\rm lat}|N\rangle$ at $m_{s,\rm phys}$ with the phenomenological estimate of D and F. Then, the fit reproduces our small values of $\langle N|\mathcal{O}_S^{\rm lat}|N\rangle$ by a large cancellation among chiral corrections at different orders. Consequently, the HBChPT expansion exhibits a poor convergence as shown in Fig. 11. A similarly poor convergence of HBChPT has been observed in our study in two-flavor QCD [8]. These observations suggest that, at least for $\langle N|\mathcal{O}_S^{\rm lat}|N\rangle$, the $SU(3)$ chiral expansion up to $O(M^2_{\{K,\eta\}})$ could be applicable only to lattice data at much smaller values of m_s.

In this study, therefore, we determine $\langle N|\mathcal{O}_S^{\rm lat}|N\rangle$ from the linear fit (29) and use the HBChPT fit only to estimate the systematic uncertainty of the chiral extrapolation. We obtain $\langle N|\mathcal{O}_S^{\rm lat}|N\rangle = 0.15(19)(18)$ from the spectrum method and 0.06(10)(10) from the ratio method. The first and second errors represent the statistical and systematic ones. In this study, the ratio method provides a statistically better determination of $\langle N|\bar{s}s|N\rangle$. This is partly because we employ a better setup of LMA for the ratio method as mentioned in Secs. II D and III C. A nucleon operator with a better overlap with the nucleon ground state also improves the accuracy of the spectrum method.

As discussed in Sec. III, we expect that the FVE on our larger volume is small. The discretization effect is estimated as $O((a\Lambda)^2) \sim 9\%$ from a simple order counting using $\Lambda = 500$ MeV. These systematic errors are well below our statistical accuracy and, hence, ignored in the following discussions. We also note that exact chiral symmetry in our simulation, forbids the mixing with the light quark contents $\langle N|\bar{u}u + \bar{d}d|N\rangle$ [7–9], which turned out to introduce a large uncertainty in $\langle N|\bar{s}s|N\rangle$ [9].

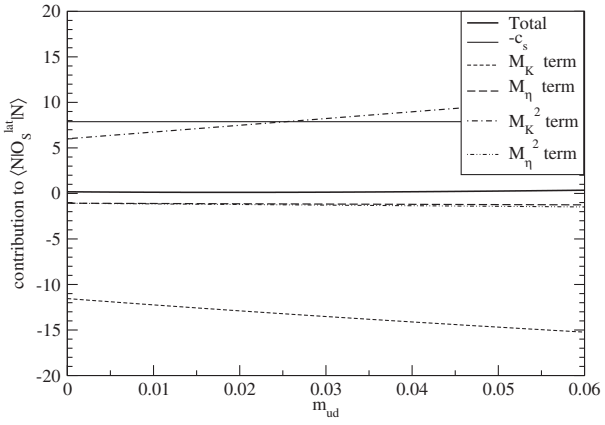

FIG. 11. Contribution to $\langle N|\mathcal{O}_S^{\rm lat}|N\rangle$ in the chiral expansion (30). Each contribution is calculated at the physical strange quark mass.

The bare matrix element $\langle N|\mathcal{O}_S^{\rm lat}|N\rangle$ is converted to the renormalization invariant parameter

$$f_{T_s} \equiv \frac{m_s\langle N|\mathcal{O}_S^{\rm lat}|N\rangle}{M_N} = \begin{cases} 0.023(29)(28) & \text{(spectrum method)}, \\ 0.009(15)(16) & \text{(ratio method)}, \end{cases} \quad (32)$$

where we use the experimental value of M_N. In Fig. 12, we compare our results of f_{T_s} with our previous estimate in $N_f = 2$ QCD [7,8]. All of our studies give consistent results for f_{T_s}. As confirmed in Fig. 13, sea strange quark loops have small effects to a renormalization invariant quantity $m_s\langle N|\mathcal{O}_S^{\rm lat}|N\rangle$ leading to the good agreement between $N_f = 2$ and $2 + 1$ QCD. As mentioned in the Introduction, our previous study using the spectrum method in $N_f = 2$ QCD [7] estimated $\langle N|\bar{s}s|N\rangle$ from the derivative $\partial M_N/\partial m_{ud,\rm sea}$ with $m_{ud,\{\rm sea,val\}}$ sending to $m_{s,\rm phys}$. This turns out to be a reasonable estimate of $\langle N|\bar{s}s|N\rangle$ because of the very mild dependence of $\langle N|\bar{s}s|N\rangle$ on $m_{\{ud,s\}}$ shown in Fig. 9 as well as the small effect of dynamical strange quark loops in Fig. 13.

Figure 12 also compares our results with recent studies in $N_f = 2 + 1$ and $2 + 1 + 1$ lattice QCD [12–18,20]. All

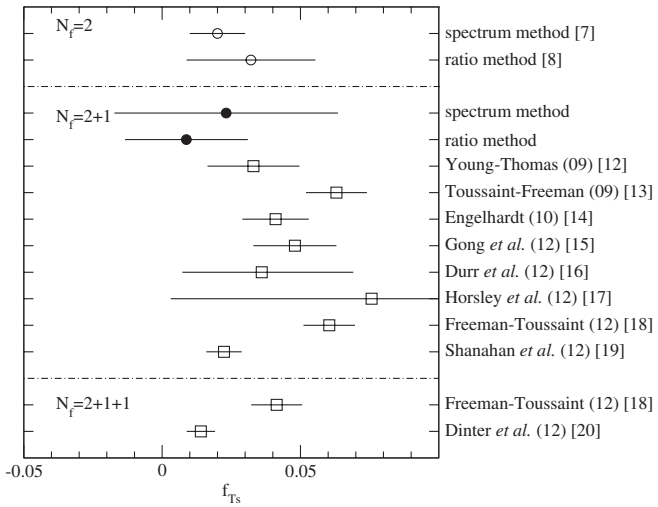

FIG. 12. Comparison of f_{T_s} with our previous studies in $N_f = 2$ QCD and recent studies in $N_f = 2 + 1$ and $2 + 1 + 1$ QCD [12–20]. We convert $m_s\langle N|\bar{s}s|N\rangle$ or $\langle N|\bar{s}s|N\rangle$ in Refs. [13,17–19] to f_{T_s} using the experimental value of M_N and m_s obtained in Ref. [41].

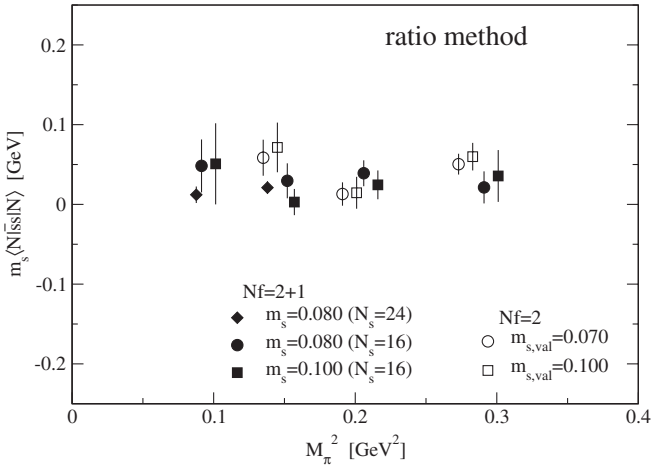

FIG. 13. A comparison of a renormalization invariant quantity $m_s\langle N|\bar{s}s|N\rangle$ between $N_f = 2$ (Ref. [8], open symbols) and $2 + 1$ (this study, filled symbols) QCD. We plot data from the ratio method as a function of M_π^2.

these studies favor small strange quark content $f_{T_s} \lesssim 0.1$. Strictly speaking, the results of Ref. [13] appears to be slightly higher (2.5σ) than our best estimate, that is f_{T_s} in $N_f = 2 + 1$ QCD from the ratio method. Recently, the same authors present improved estimates in $N_f = 2 + 1$ and $2 + 1 + 1$ QCD [18]. These results also indicate a slightly large value of $f_{T_s} \sim 0.06$. Given the large statistical errors, however, the difference is not very significant.

Compared to these lattice estimates, the phenomenological studies [2,3] predict a rather large estimate 0.41 (9) based on HBChPT up to quadratic order in the quark masses. The poor convergence of our chiral fit based on the same effective theory suggests that its convergence at physical quark masses should be carefully examined.

V. CONCLUSION

In this paper, we calculate the strange quark content of the nucleon in $2 + 1$-flavor lattice QCD. Two determinations using the ratio and spectrum methods as well as our previous studies in two-flavor QCD consistently favor a small strange quark content $f_{T_s} \lesssim 0.05$. In contrast, phenomenological studies based on HBChPT have led to a rather larger value 0.1–0.7 which is, however, unexpectedly large as a content of sea quarks of a single flavor.

In this study, we utilize several simulation techniques to precisely determine the small effect due to disconnected quark loops. In the spectrum method, we can successfully shift m_s by ± 25 MeV by using the reweighting technique. It would be interesting to study isospin breaking effects, such as the proton and neutron mass difference, by using this technique, and its applicability on larger lattice volumes should be studied.

The ratio method requires precise calculation of the nucleon disconnected three-point function, which is technically very challenging. The low-lying modes of the Dirac operator turned out to be very helpful: we employ the LMA technique to calculate the nucleon propagator and the all-to-all quark propagator for the disconnected quark loops. These techniques, in principle, can be applied to other baryon observables. For instance, it is interesting to extend this study to the strange quark spin content of the nucleon. Precise knowledge of this quantity is important to constrain the parameter space of SUSY models through spin-dependent scattering cross section of the neutralino-nucleon scattering [40].

ACKNOWLEDGMENTS

Numerical simulations are performed on Hitachi SR11000 and IBM System Blue Gene Solution at High Energy Accelerator Research Organization (KEK) under a support of its Large Scale Simulation Program (No. 06-13, 07-16, 08-05, 09-05, 09/10-09, and 10-11) as well as on NEC SX-8 and Hitachi SR16000 at YITP, Kyoto University and NEC SX-8R at RCNP, Osaka University. This work is supported in part by Grant-in-aid for Scientific Research of Japan (Grants No. 18340075, No. 20105001, No. 20105002, No. 20105005, No. 21674002, No. 21684013, No. 22224003) and Grant-in-Aid for Scientific Research on Innovative Areas (Grants No. 2004: 20105001, No. 20105002, No. 20105003, No. 20105005).

[1] T. Falk, A. Ferstl, and K. A. Olive, Phys. Rev. D **59**, 055009 (1999); **60**, 119904(E) (1999).
[2] M. M. Pavan *et al.*, PiN Newslett. **16**, 110 (2002).
[3] B. Borasoy and U.-G. Meissner, Ann. Phys. (N.Y.) **254**, 192 (1997).
[4] M. Fukugita, Y. Kuramashi, M. Okawa, and A. Ukawa, Phys. Rev. D **51**, 5319 (1995).
[5] S. J. Dong, J. F. Lagae, and K. F. Liu, Phys. Rev. D **54**, 5496 (1996).
[6] S. Güsken, P. Ueberholz, J. Viehoff, N. Eicker, P. Lacock, T. Lippert, K. Schilling, A. Spitz, and T. Struckmann (SESAM Collaboration), Phys. Rev. D **59**, 054504 (1999).
[7] H. Ohki, H. Fukaya, S. Hashimoto, T. Kaneko, H. Matsufuru, J. Noaki, T. Onogi, E. Shintani, and N. Yamada, Phys. Rev. D **78**, 054502 (2008).
[8] K. Takeda, S. Aoki, S. Hashimoto, T. Kaneko, J. Noaki, and T. Onogi (JLQCD Collaboration), Phys. Rev. D **83**, 114506 (2011).

[9] C. Michael, C. McNeile, and D. Hepburn (UKQCD Collaboration), Nucl. Phys. B, Proc. Suppl. **106**, 293 (2002).

[10] G. S. Bali *et al.* (QCDSF Collaboration), Phys. Rev. D **85**, 054502 (2012).

[11] R. Babich, R. C. Brower, M. A. Clark, G. T. Fleming, J. C. Osborn, C. Rebbi, and D. Schaich, Phys. Rev. D **85**, 054510 (2012).

[12] R. D. Young and A. W. Thomas, Phys. Rev. D **81**, 014503 (2010).

[13] D. Toussaint and W. Freeman (MILC Collaboration), Phys. Rev. Lett. **103**, 122002 (2009).

[14] M. Engelhardt, Proc. Sci., LATTICE2010 (2010) 137.

[15] M. Gong *et al.* (χQCD Collaboration), Proc. Sci., LATTICE2011 (2011) 156.

[16] S. Dürr, Z. Fodor, T. Hemmert, C. Hoelbling, J. Frison, S. D. Katz, S. Krieg, T. Kurth *et al.*, Phys. Rev. D **85**, 014509 (2012).

[17] R. Horsley, Y. Nakamura, H. Perlt, D. Pleiter, P. E. L. Rakow, G. Schierholz, A. Schiller, H. Stüben, F. Winter, and J. M. Zanotti, Phys. Rev. D **85**, 034506 (2012).

[18] W. Freeman and D. Toussaint (MILC Collaboration), arXiv:1204.3866.

[19] P. E. Shanahan, A. W. Thomas, and R. D. Young, arXiv:1205.5365.

[20] S. Dinter, V. Drach, R. Frezzotti, G. Herdoiza, K. Jansen, and G. Rossi, J. High Energy Phys. 08 (2012) 037.

[21] H. Neuberger, Phys. Lett. B **417**, 141 (1998).

[22] H. Neuberger, Phys. Lett. B **427**, 353 (1998).

[23] H. Ohki *et al.* (JLQCD Collaboration), Proc. Sci., LAT2009 (2009) 124.

[24] K. Takeda *et al.* (JLQCD Collaboration), Proc. Sci., LATTICE2010 (2010) 160.

[25] S. Aoki *et al.* (JLQCD Collaboration), Phys. Rev. D **78**, 014508 (2008).

[26] Y. Iwasaki, Report No. UTHEP-118, 1983 (unpublished).

[27] H. Fukaya, S. Hashimoto, K. I. Ishikawa, T. Kaneko, H. Matsufuru, T. Onogi, and N. Yamada (JLQCD Collaboration), Phys. Rev. D **74**, 094505 (2006).

[28] S. Aoki, H. Fukaya, S. Hashimoto, and T. Onogi, Phys. Rev. D **76**, 054508 (2007).

[29] J. Noaki *et al.* (JLQCD Collaboration), Proc. Sci., LATTICE2010 (2010) 117.

[30] J. Noaki *et al.* (JLQCD Collaboration) (to be published).

[31] G. S. Bali, H. Neff, T. Dussel, T. Lippert, and K. Schilling (SESAM Collaboration), Phys. Rev. D **71**, 114513 (2005).

[32] J. Foley, K. J. Juge, A. O'Cais, M. Peardon, S. M. Ryan, and J. I. Skullerud, Comput. Phys. Commun. **172**, 145 (2005).

[33] S.-J. Dong and K.-F. Liu, Phys. Lett. B **328**, 130 (1994).

[34] T. A. DeGrand and S. Schaefer, Comput. Phys. Commun. **159**, 185 (2004).

[35] L. Giusti, P. Hernandez, M. Laine, P. Weisz, and H. Wittig, J. High Energy Phys. 04 (2004) 013.

[36] T. DeGrand, Phys. Rev. D **78**, 117504 (2008).

[37] A. Hasenfratz, R. Hoffmann, and S. Schaefer, Phys. Rev. D **78**, 014515 (2008).

[38] A. Walker-Loud, Nucl. Phys. **A747**, 476 (2005).

[39] E. E. Jenkins and A. V. Manohar, Phys. Lett. B **259**, 353 (1991).

[40] J. R. Ellis, K. A. Olive, and C. Savage, Phys. Rev. D **77**, 065026 (2008).

[41] A. Bazavov *et al.* (MILC Collaboration), Proc. Sci., LAT2009 (2009) 079.